X-622-67-471

NASA TM X-55958

THE REMOTE SENSING OF STRATOSPHERIC TEMPERATURES AND SOME RESULTS FROM THE NIMBUS II SATELLITE EXPERIMENT

GUENTER WARNECKE

SEPTEMBER 1967

GODDARD SPACE FLIGHT CENTER
GREENBELT, MARYLAND

X-622-67-471

THE REMOTE SENSING OF STRATOSPHERIC TEMPERATURES AND SOME RESULTS FROM THE NIMBUS II SATELLITE EXPERIMENT

Guenter Warnecke

(Lecture given at the "STANSTEAD SEMINARS ON THE MIDDLE ATMOSPHERE 1967" held by Meteorology Department, McGill University, Montreal at the Stanstead College, Stanstead, P. Q., Canada from July 24 to August 5, 1967)

September 1967

GODDARD SPACE FLIGHT CENTER
Greenbelt, Maryland

THE REMOTE SENSING OF STRATOSPHERIC TEMPERATURES AND SOME RESULTS FROM THE NIMBUS II SATELLITE EXPERIMENT

Guenter Warnecke*
Goddard Space Flight Center

ABSTRACT

The Nimbus II medium resolution infrared radiometer measured atmospheric radiation in five spectral regions. Radiance measurements in a two-micron-wide spectral interval within the 15 micron carbon dioxide band permitted the derivation of vertically averaged stratospheric temperatures and made possible the daily monitoring of global stratospheric temperature patterns. The experiment lasted from May 15 through July 28, 1966. For this period, stratospheric temperature maps were produced by a computer program which included a method to eliminate the effect of dense high clouds on the 14 to 16 micron measurements. The method of measurement, the applied correction model, and some results of the Nimbus II experiment are described.

Due to the seasonal restriction of the experiment, the derived global stratospheric temperature distributions exhibit the most interesting events over the southern hemisphere, where the southern polar winter vortex shows a pronounced asymmetry during the early winter of 1966. Within the 70 days of observation, this asymmetry travels around the South Pole and finally vanishes. The resultant horizontal cooling pattern seems to emphasize the important role of dynamic processes in the net cooling of the polar winter stratosphere.

*On leave from the Freie Universitaet Berlin, Germany, as a National Academy of Sciences – National Research Council Senior Postdoctoral Resident Research Associate with the National Aeronautics and Space Administration.

CONTENTS

ILLUSTRATIONS

ILLUSTRATIONS (Continued)

THE REMOTE SENSING OF STRATOSPHERIC TEMPERATURES AND SOME RESULTS FROM THE NIMBUS II SATELLITE EXPERIMENT

INTRODUCTION

One of the serious problems in stratospheric meteorology is the lack of continuous observational data over large parts of the globe. Figure 1 represents the effective global network of radiosonde measurements at the 30 mb (approx. 25 km) and the 10 mb (approx. 30 km) levels on a single day in January 1964. There has been little change since that time. It should be noticed that a barely sufficient network density exists only over the northern hemispheric continents while over the oceans, the tropics, subtropics, and almost the entire southern hemisphere we suffer a severe lack of information.

A satellite in a quasi-polar orbit provides an excellent platform for complete observation of the earth (Ref. 1). Radiometric experiments on board the TIROS VII and Nimbus II satellites have shown that measurements of the atmospheric emission within the 15 micron carbon dioxide band can provide information on the stratospheric temperature structure[2][3], as was first suggested by KAPLAN (4).

In this presentation, the method of radiometric measurement and data reduction and also the interpretation of the Nimbus II experiment will briefly be discussed.

THE THEORETICAL BACKGROUND OF REMOTE SENSING TECHNIQUES

The thermal radiation leaving the earth-atmosphere system at the top of the atmosphere (satellite altitude) and measured through a filter system can be described by the radiative transfer equation, if blackbody radiation is assumed, in the form

$$N = \frac{1}{\pi}\int_{\lambda_1}^{\lambda_2} \Phi(\lambda)\,\tau_s(\lambda)\,B\left(\lambda, T_s\right)\,d\lambda + \frac{1}{\pi}\int_{\lambda_1}^{\lambda_2}\int_{h=0}^{h} \Phi(\lambda)\,\frac{\partial\tau(\lambda, h)}{\partial h}\,B\left(\lambda, T(h)\right)\,dh\,d\lambda \qquad (1)$$

where N is the detected radiance; λ = wavelength; $\Phi(\lambda)$ is the filter function, $\Phi(\lambda) = 0$ outside the interval $\{\lambda_1, \lambda_2\}$; $\tau(\lambda, h)$ = transmissivity from a level h upward; τ_s = transmissivity from the radiating surface upward; $B(\lambda, T)$ = Planck

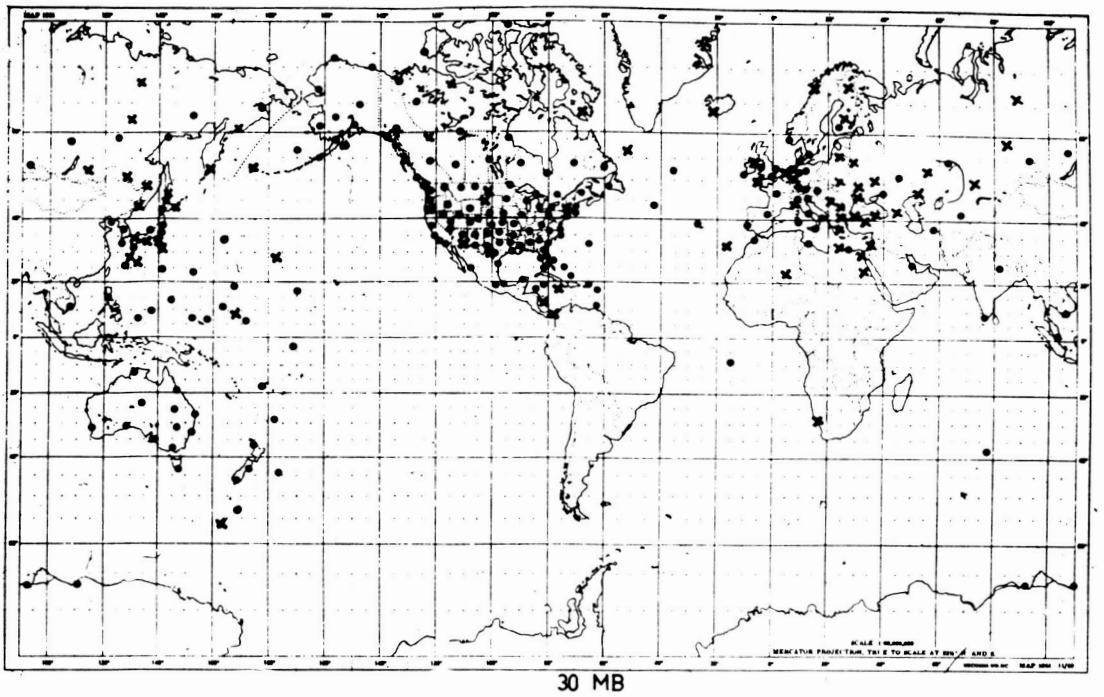

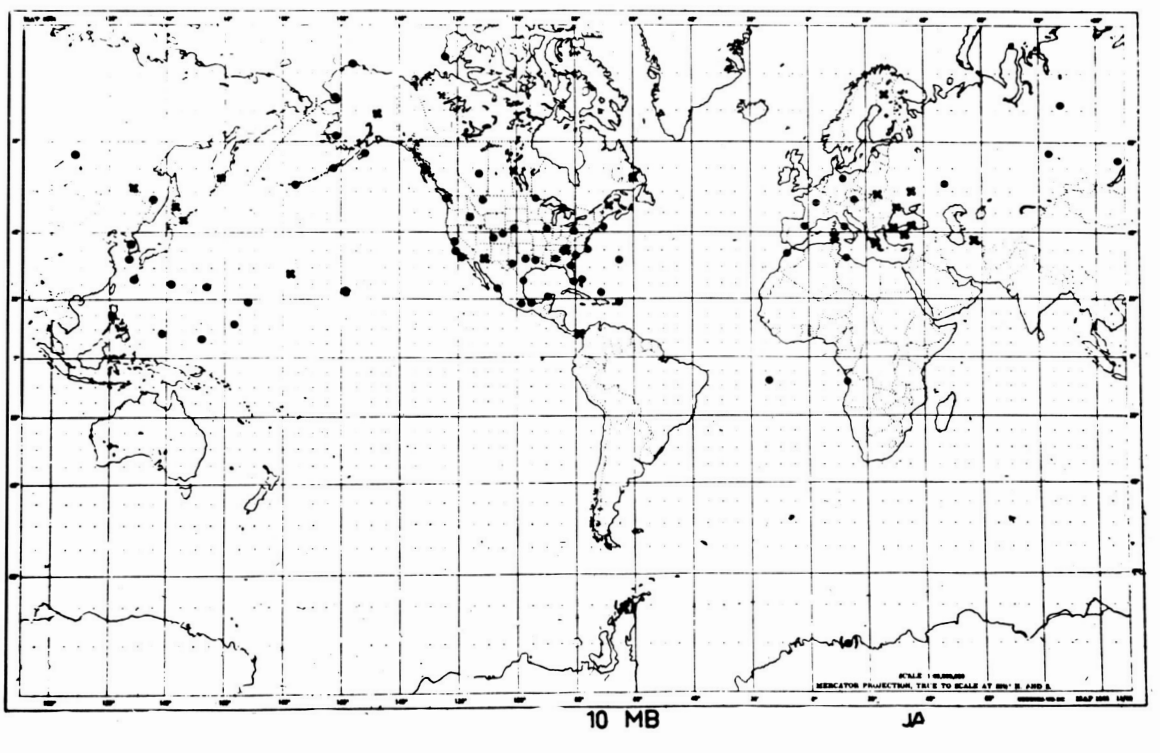

Figure 1. Available global radiosonde observations at the 30 mb and 10 mb levels on January 22, 1964, 00 GMT (x = 12 GMT, ( ) = wind observations only).

function; T = absolute temperature; T_s = temperature of the radiating surface; and h = height. The first term on the right side of this equation describes the contribution of surfaces, both solid and liquid (such as the earth and clouds), to the recorded radiance; the second term describes the radiation originating from the gaseous compounds of the atmosphere.

By the use of Equation (1) structural parameters of the atmosphere can be derived from a radiometric measurement of N under two different special conditions:

(a) In an atmospheric "window" (if the atmosphere were completely transparent, i.e., $\tau_s(\lambda) = 1$) the second term on the right side of Equation (1) equals zero. Thus Equation (1) becomes

$$N_w = \frac{1}{\pi} \int_{\lambda_1}^{\lambda_2} \Phi(\lambda)\, B\left(\lambda, T_s\right)\, d\lambda \qquad (2)$$

With $\Phi(\lambda)$ being known, the measured radiance depends on the only unknown variable, i.e., the temperature T of the radiating surface. If the radiometer is calibrated against a black body radiator, the recorded radiance readily can be converted to 'equivalent blackbody temperature' (5). This means—in meteorological terms—the earth surface temperature or in cloudy areas the cloud top temperature could be derived from radiometric measurements in an atmospheric "window." It should be pointed out here that the surface emissivity is considered to be unity due to the assumption of blackbody radiation in Equation (1). This does not hold for natural conditions, but with regard to the spectral "window" region the error resulting from this assumption lies within the noise region of the entire method. Experiments of this type were very successfully flown on the TIROS II, III, IV, VII, and Nimbus I and II meteorological satellites leading to detailed and global pictures of horizontal and vertical cloud distribution as well as a mapping of sea surface and land temperatures under clear sky conditions.

(b) In a strong absorption band of one of the predominant atmospheric absorbers like carbon dioxide, water vapor or ozone, where the transmission from the ground is zero, the first term of Equation (1) vanishes, leading to

$$N_A = \frac{1}{\pi} \int_{\lambda_1}^{\lambda_2} \int_{h=0}^{h} \Phi(\lambda)\, \frac{\partial \tau(\lambda, h)}{\partial h}\, B\left(\lambda, T(h)\right)\, dh\, d\lambda \qquad (3)$$

In this case, N is determined by two unknown variables, namely $\partial\tau/\partial h$, which characterizes the vertical gas distribution, and $B(\lambda, T)$, which depends on the averaged gas temperature. One of these two factors has to be known in order to interpret N in terms of the other one. In principal, inferences of the horizontal distribution of the highly variable gases (water vapor and ozone) are possible, if the three-dimensional temperature distribution in the atmosphere can be given. Experiments of this type were performed in the 6.3 to 6.7 micron water vapor band with the TIROS II, III, IV, and Nimbus II satellites, leading to quasi-global horizontal distributions of water vapor in the upper troposphere, see for example (13).

The second possibility, namely the derivation of the vertical mean temperature if the gas distribution is known, was successfully accomplished by TIROS VII and Nimbus II experiments[2][3] for the well-mixed atmospheric carbon dioxide, which has a strong absorption band at 15 micron.

THE INTERPRETATION OF RADIANCE MEASUREMENTS WITHIN THE 15 MICRON BAND

From Equation (3) follows that N_A can be expressed as

$$N_A = \frac{1}{\pi} \int_{h=0}^{h} \Psi(h)\, dh \tag{4}$$

where

$$\Psi(h) = \int_{\lambda_1}^{\lambda_2} \Phi(\lambda)\, B\big(\lambda, T(h)\big)\, \frac{\partial\tau(\lambda, h)}{\partial h}\, d\lambda \tag{5}$$

describes the variation with height of the contribution of the individual atmospheric layers to the 15 micron radiation detected by the satellite radiometer.

This weighting function has a maximum in the lower stratosphere. Due to the increasing gas density with decreasing height, the emitted energy per unit volume increases downward. Below a certain altitude less and less radiation penetrates upward because of the absorption in the overlying layers.

The temperature to be derived from Equation (3) is therefore a weighted mean temperature, weighted over the entire carbon dioxide atmosphere with the function $\Psi(h)$.

The weighting function $\Psi(h)$ depends—among other things—on the filter function $\Phi(h)$. This is illustrated by Figures 2 and 3 where the filter functions

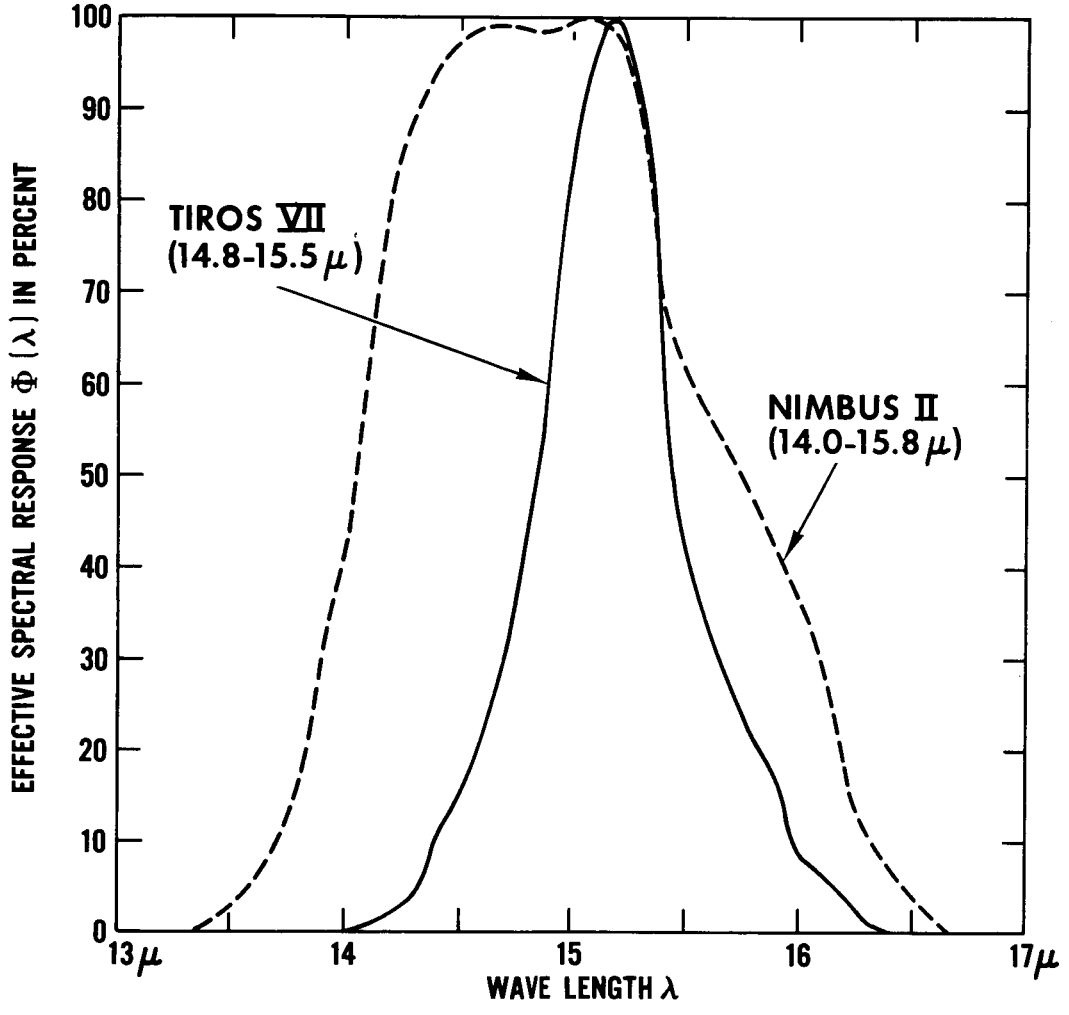

Figure 2. Normalized filter functions $\Phi(\lambda)$ of the 15 micron channels of the TIROS VII and Nimbus II Medium Resolution Radiometers.

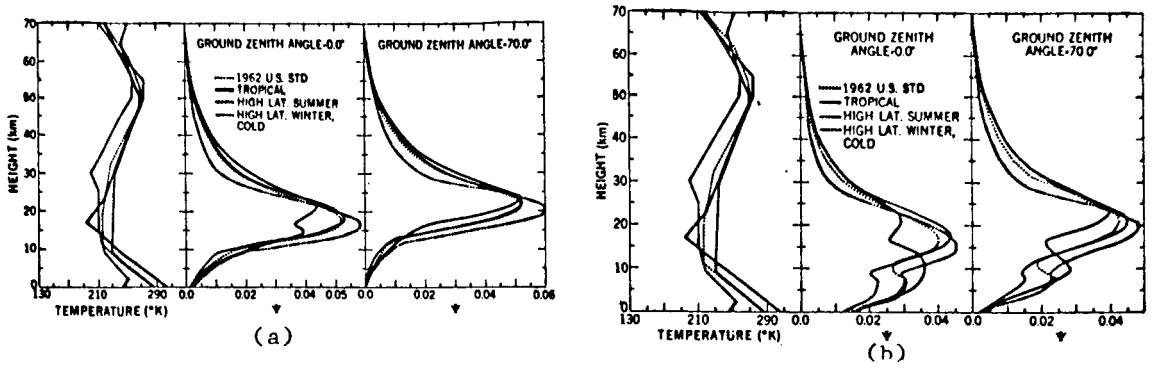

Figure 3. Weighting functions $\Psi(h)$ for different atmospheres for the TIROS VII and Nimbus II filter response (after V. Kunde (6)).

and resulting weighting functions for various atmospheres are given for the TIROS VII and Nimbus II 15 micron radiometer channels.

The wider filter spectral range of the Nimbus II radiometer results in a lower altitude of the maximum contribution and in a much larger tropospheric contribution to the recorded radiance, as compared with TIROS VII. How much $\Psi(h)$ depends on the atmospheric structure, is shown in Figure 3. For all the atmospheres, the weighting function peaks in the lower stratosphere, which means that the measured horizontal distribution of outgoing radiance should reflect the horizontal temperature distribution within this layer.

The radiometer is calibrated against a blackbody of known temperature (5). Thus, the measured radiances can be interpreted in terms of the temperature of a blackbody of the same radiance ("equivalent blackbody temperature" T_{BB}):

$$N_A = \frac{1}{\pi} \int_{\lambda_1}^{\lambda_2} \Phi(\lambda)\, B\left(\lambda, T_{BB}\right) d\lambda \qquad (6)$$

The "equivalent blackbody temperature" then represents—as mentioned before—the weighted vertical mean temperature of the atmosphere, with $\Psi(h)$ as the weighting function.

From the TIROS VII measurements, it has been shown that stratospheric temperature distributions can be derived from 15 micron radiometry (2) (7) (8). It has also been shown that a high correlation exists between radiosonde-derived hemispheric patterns of 30 mb temperatures (9) (10) and 10 mb/100 mb thickness

patterns (vertical mean temperatures) (11) on the one hand and satellite derived stratospheric temperatures (T_{BB}) on the other.

The interpretation of the derived equivalent blackbody temperature as vertical mean stratospheric temperature, however, holds exactly only in a gaseous atmosphere, i.e., in the absence of clouds. If sufficiently dense clouds do exist within the altitude range of $\Psi(h)$, radiation from below the clouds does not penetrate to the satellite. This will cause a reduction of the outgoing radiance because a tropospheric cloud itself radiates with a lower temperature than the atmosphere below it. The effect will be larger for higher clouds. Figure 3 demonstrates how much the cloud effect will depend on the filter properties of the instrument. While in the case of TIROS VII only a small percentage of tropospheric radiation passes the filter of the radiometer, in the case of Nimbus II 15 to 20% came from below the tropopause, and a very significant effect of dense high cloud systems on the 15 micron measurements resulted.

Figure 4 shows a photofacsimile display of the medium resolution radiometer measurements along parts of Nimbus II orbit 344/5 on June 10, 1966. In this figure, taken from the Nimbus II Pictorial Data Catalog (12), high radiation intensities (high temperatures) are represented by dark grey tones, low intensities (low temperatures) by light grey or white. In the case of the 10-11 micron (atmospheric "window") measurements of Figure 4, the bright areas indicate a number of cloud systems of various sizes and at different geographic locations. The photographic imagery of the 14-16 micron measurements, which shows well discernable grey tones from the darker (warm) Arctic toward the brighter (cold) Antarctic stratosphere, exhibits, however, a considerable "background noise." The cloud pattern of the "window" channel clearly appears superimposed upon the stratospheric temperature distribution. Therefore, the cloud effect has to be eliminated before stratospheric temperature distributions can be derived from the measurements. A method to accomplish the elimination of the cloud effect will be described in the following section.

THE ELIMINATION OF THE CLOUD EFFECT ON THE NIMBUS II 15 MICRON MEASUREMENTS

The basic concept of the method to eliminate the cloud effect from the Nimbus II 15 micron measurements was first to determine the cloud effect from theoretical computations of the outgoing radiance under various atmospheric conditions and second to apply the proper correction to each single measurement using simultaneous "window" channel measurements to derive the needed actual cloud top height.

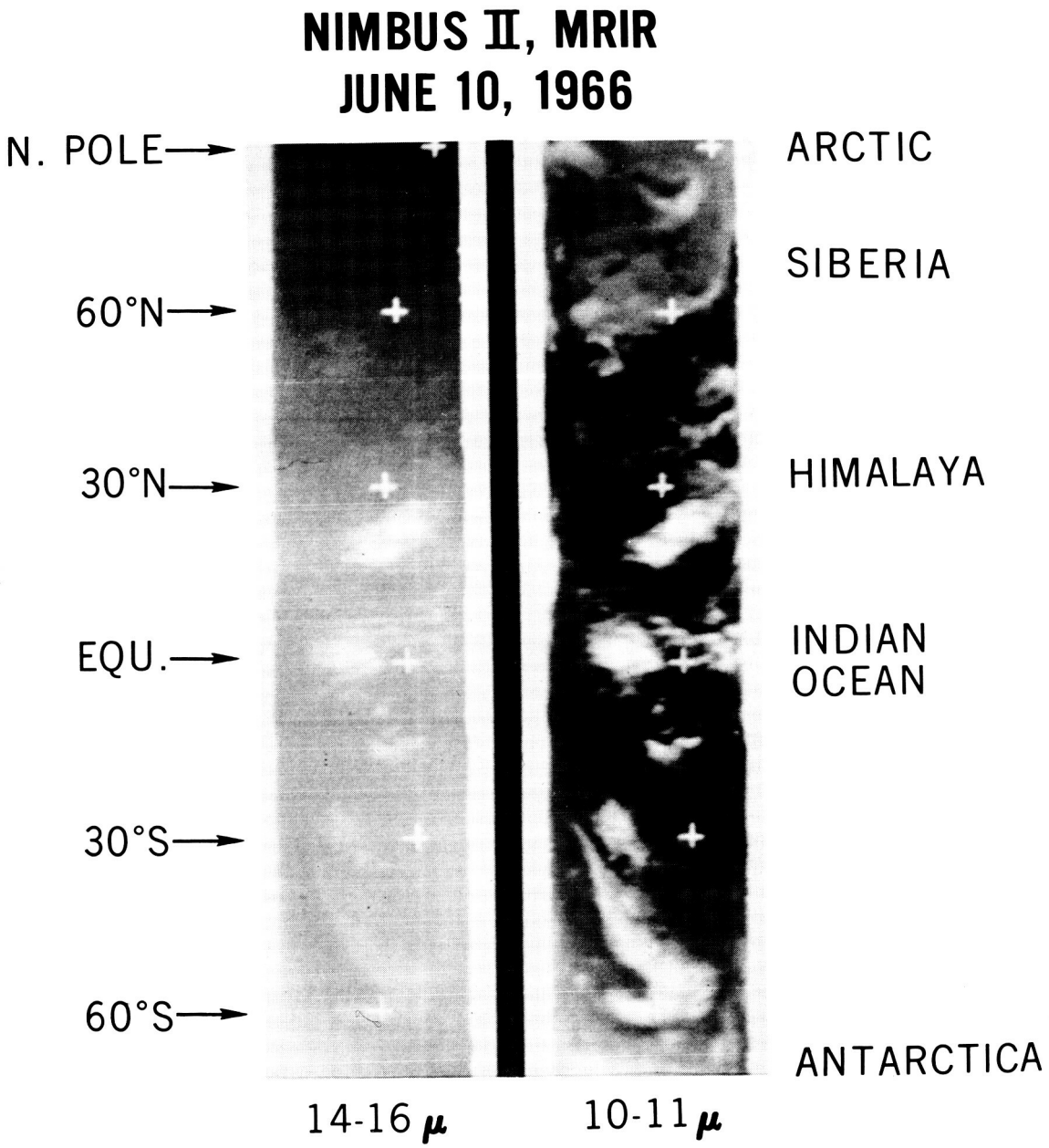

Figure 4. Photofacsimile of Medium Resolution Infrared Radiometer (MRIR) measurements (Nimbus II) in the "Window" and carbon dioxide channels.

The outgoing infrared radiation for 7 atmospheres (different months and latitudes) and various nadir angles within the Nimbus II 15 micron filter range was computed from the radiative transfer equation for clear sky conditions and cloud decks assumed at various altitudes using a computer program developed

by V. Kunde (6). This yielded a quantitative measure for the cloud effect. The computations showed that the cloud effect is almost the same for all atmospheres up to cloud top heights of 10 kilometers. Above this height, however, large differences occur for different geographic areas and seasons. Figures 5 and 6 are examples for strong and weak effects of these high cloud systems. While for a cloud top at 10 kilometers in both cases the depression of the derived T_{BB} value is close to 4°K for vertical view, it increases to only 5°K in the 45°N winter atmosphere at 14 kilometers but to 11°K at the same altitude in the tropics.

The cloud effect was computed for the 15°, 30°, 45°, and 60°N U. S. Standard Atmospheres and was determined for every month and scan nadir angle. However,

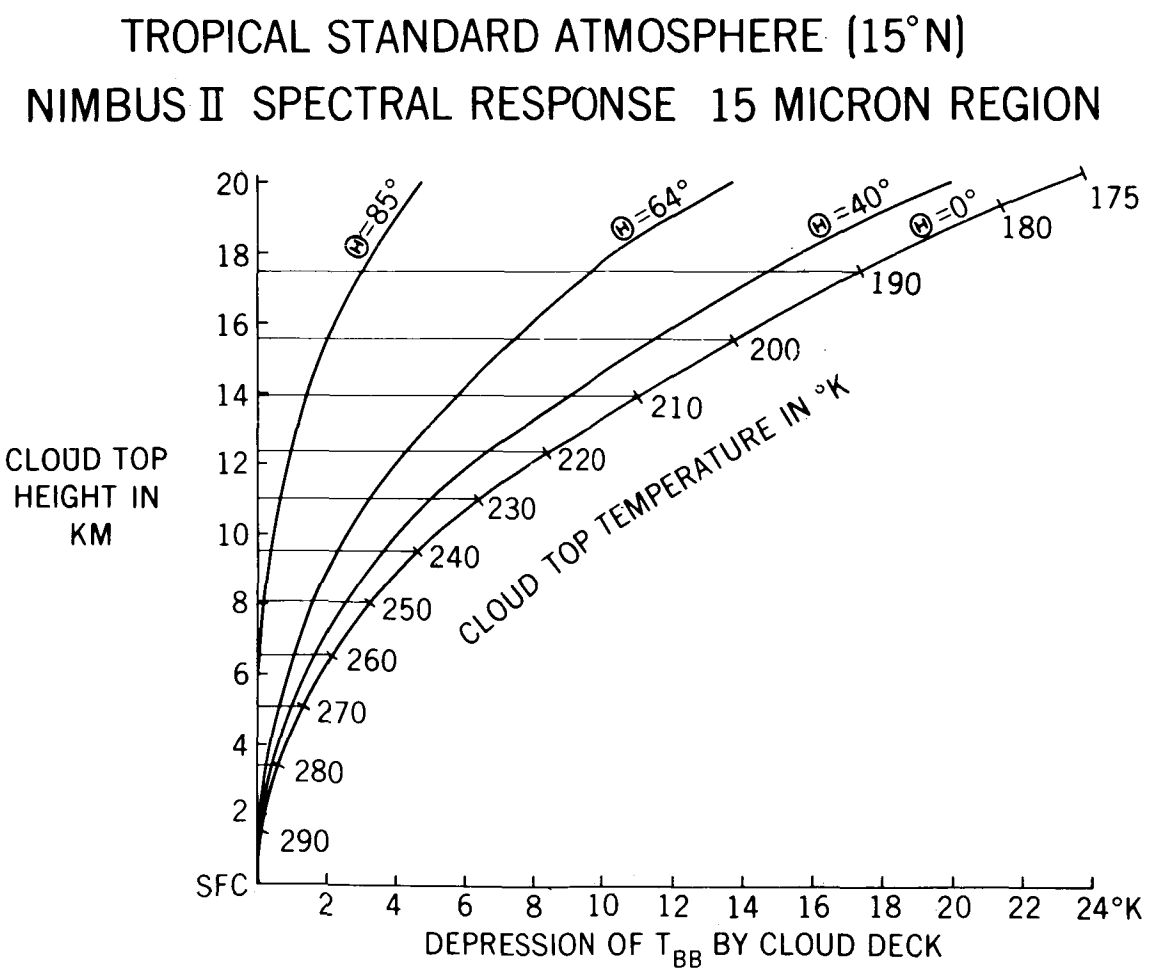

Figure 5. Effect of an opaque cloud deck filling the field of view of the Nimbus II radiometer on the measured equivalent blackbody temperature (T_{BB}) of the carbon dioxide channel (Θ = ground zenith angle) in a tropical atmosphere.

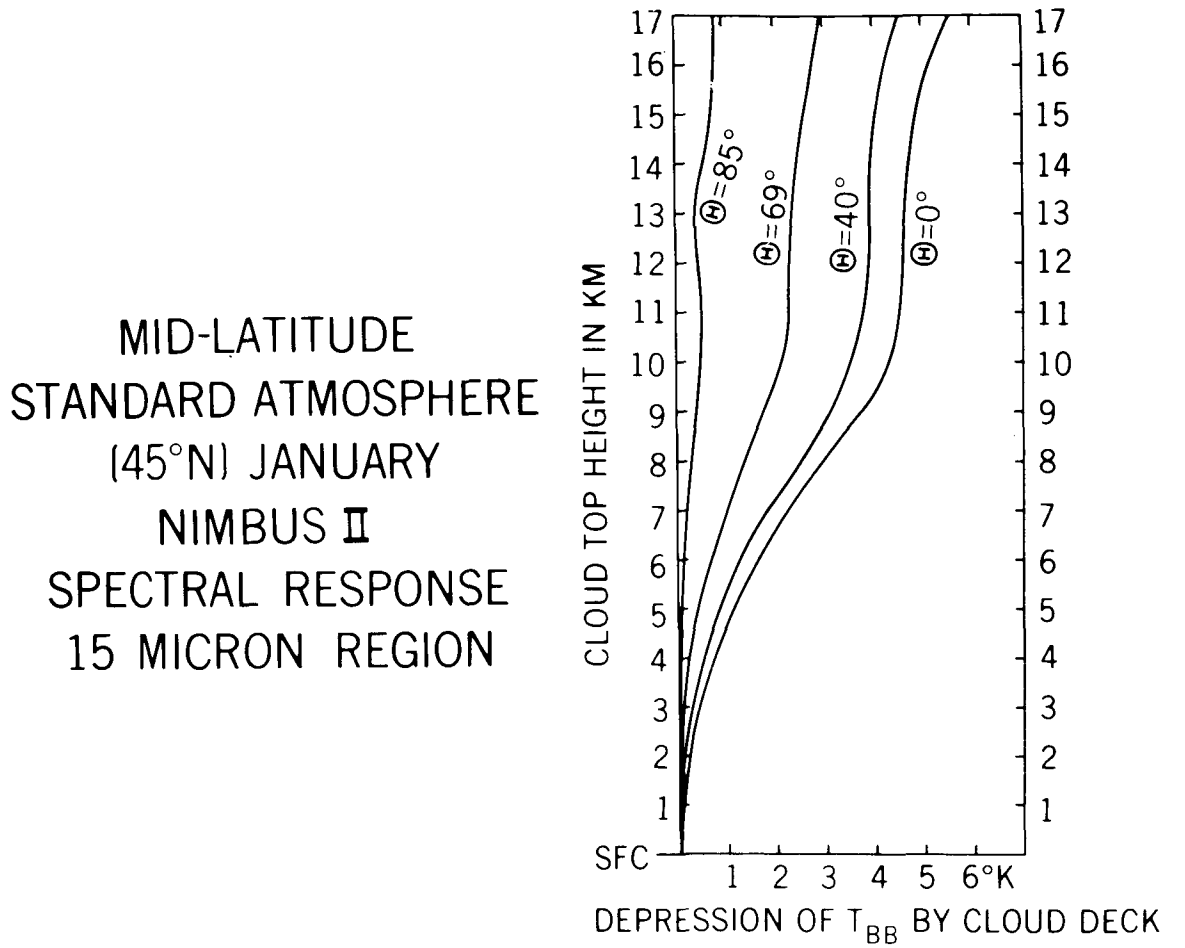

Figure 6. Effect of an opaque cloud deck filling the field of view of the Nimbus II radiometer on the measured equivalent blackbody temperature (T_{BB}) of the carbon dioxide channel in a mid-latitude winter atmosphere (Θ = ground zenith angle).

before applying these computed amounts to the measurements the actual cloud top heights have to be derived from the "window" channel measurements. As the 10-11 micron "window" is not completely free of atmospheric absorption, corrections have to be made for residual water vapor and ozone absorption. These corrections were computed from the radiative transfer equation for the Nimbus II 10-11 micron filter range and the same group of atmospheres. One example of the results is given in Figure 7. From this diagram the cloud top temperature can be obtained for any measured equivalent blackbody temperature in a tropical atmosphere. From the obtained cloud top temperature, cloud top height can be derived for the proper temperature-height relationship. In Figure 8, this relationship has been built in, thus the correction of the 15 micron channel measurement can readily be taken from this diagram.

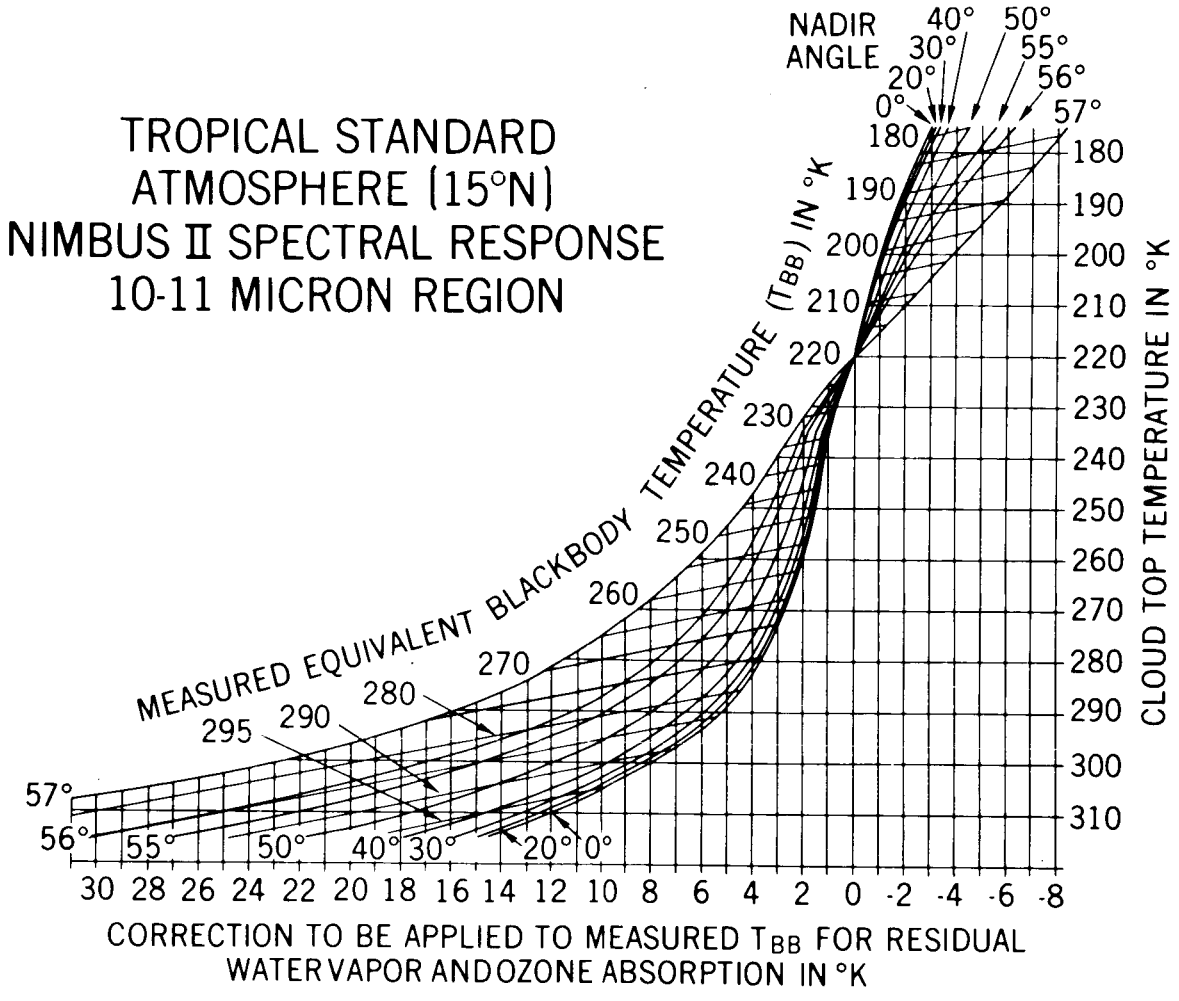

Figure 7. Diagram to correct the Nimbus II MRIR "window" channel measurements for residual water vapor and ozone absorption in a tropical atmosphere.

On the basis of the described model calculations, a computer program was developed:

(a) to determine for each single observation the cloud top height from the concurrent "window" channel measurement and, with this information,

(b) to apply the proper correction to the 15 micron channel measurement.

THE PRODUCTION OF NIMBUS II STRATOSPHERIC TEMPERATURE MAPS

The Nimbus II medium resolution infrared radiometer experiment lasted from May 15 through July 28, 1966. The orbital inclination of 100 degrees and

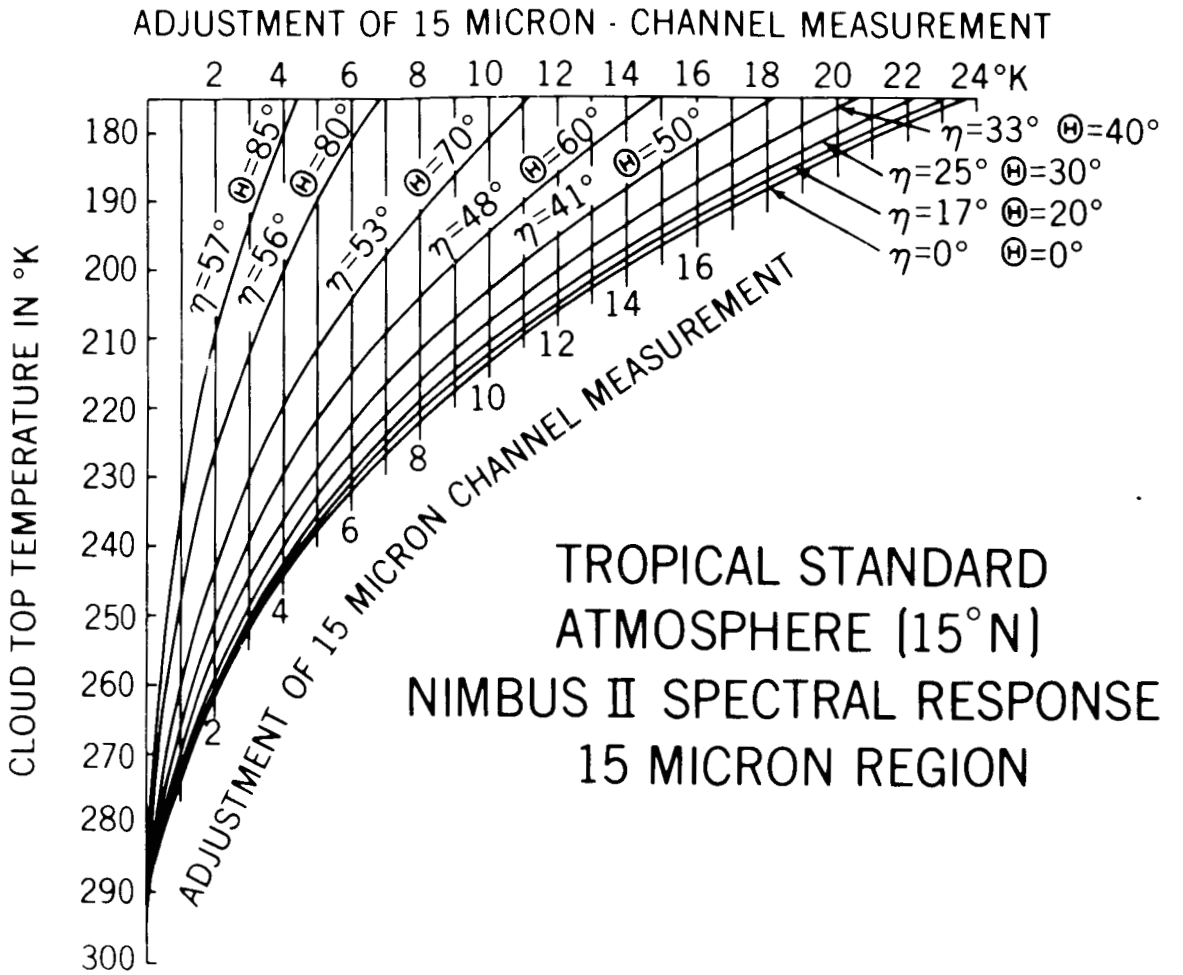

Figure 8. Diagram to correct the Nimbus II MRIR CO_2 channel measurements for cloud contamination in a tropical atmosphere (η = nadir angle, Θ = ground zenith angle).

the average satellite altitude of approximately 1100 km provided a complete scanning of the globe. The two medium resolution radiometer channels (3 degrees field of view) used for this analysis were sensitive in the 14 to 16 micron (carbon dioxide band) and in the 10 to 11 micron ("window") spectral regions. This is described in more detail elsewhere (5).

After the elimination of cloud contamination, the corrected measurements were automatically mapped by an electronic computer and printed in 1:40 million Mercator and polar stereographic projections. Figure 9 is a typical example of such a computer printout, exhibiting the data taken in a 24 hour period over the globe. The "contouring method" was used in the printing process in order to give automatically a pattern analysis of the data.

Figure 9. Typical example of a computer printout in polar stereographic projection covering the southern hemisphere from the South Pole (at the center of the map) to approximately 40° S. Contouring is applied in 10°K intervals. The irregularities in the upper left and the lower center portion of the map are caused by some missing data. The geographic outlines are as in the following figures.

For this presentation, the global measurements were produced in approximately 10 day intervals. But, contrary to the TIROS VII experiment, daily maps could be analyzed without difficulties, as the signal-to-noise-ratio was considerably improved by the wide spectral response of the Nimbus II instrument. According to the season of this experiment, the northern hemisphere and the tropics do not exhibit significant structural changes during the period of May through July, 1966. Therefore, the following discussion will concentrate mainly on the southern hemisphere which was in its late fall and early winter season. It is worthwhile emphasizing that Nimbus II provided for the first time a really global picture of the stratospheric temperature distribution, including the southern polar region (3) where information is the most incomplete by conventional means and is the most needed for stratospheric research.

STRATOSPHERIC CIRCULATION FEATURES REVEALED FROM THE NIMBUS II MEASUREMENTS

The following discussion refers to Figures 10 to 20. During the period of the Nimbus II experiment, the northern hemisphere passed the climax of its warm summer circulation. The temperature distribution did not show any drastic changes. The warmest air was always located over the Arctic Ocean. Weak temperature gradients persisted all over the hemisphere. The temperature maximum occurred around July 1, 1966, with 240°K over the North Pole.

The temperature distribution over the tropics was characterized by temperatures mainly from 220 to 225°K between 30°N and 30°S with a very slight north-to-south temperature gradient. No significant temperature changes could be noticed during the period under investigation.

The southern hemisphere exhibited the more interesting events. On May 21, 1966, the southern polar vortex was already well established over the South Pole where it remained throughout the period of observation. The temperature structure of the polar vortex had, however, a remarkable asymmetry during the first six weeks. On May 21, extended areas of warm air over the southern South Atlantic and the southern Indian Ocean caused a zone of remarkably strong meridional temperature gradient. During the following twenty days, an eastward motion of the warm centers was observed. Thus, on June 10, the warm air arrived over Australia and the western South Pacific Ocean. During the second half of June, however, the warm air retreated to lower latitudes, and the polar vortex became thermally more symmetric, although a number of short waves were found to travel around the vortex center. This situation persisted throughout July, 1966.

The center of the southern polar vortex, although almost stationary during the ten-week period, was gradually cooling. From approximately 205°K around

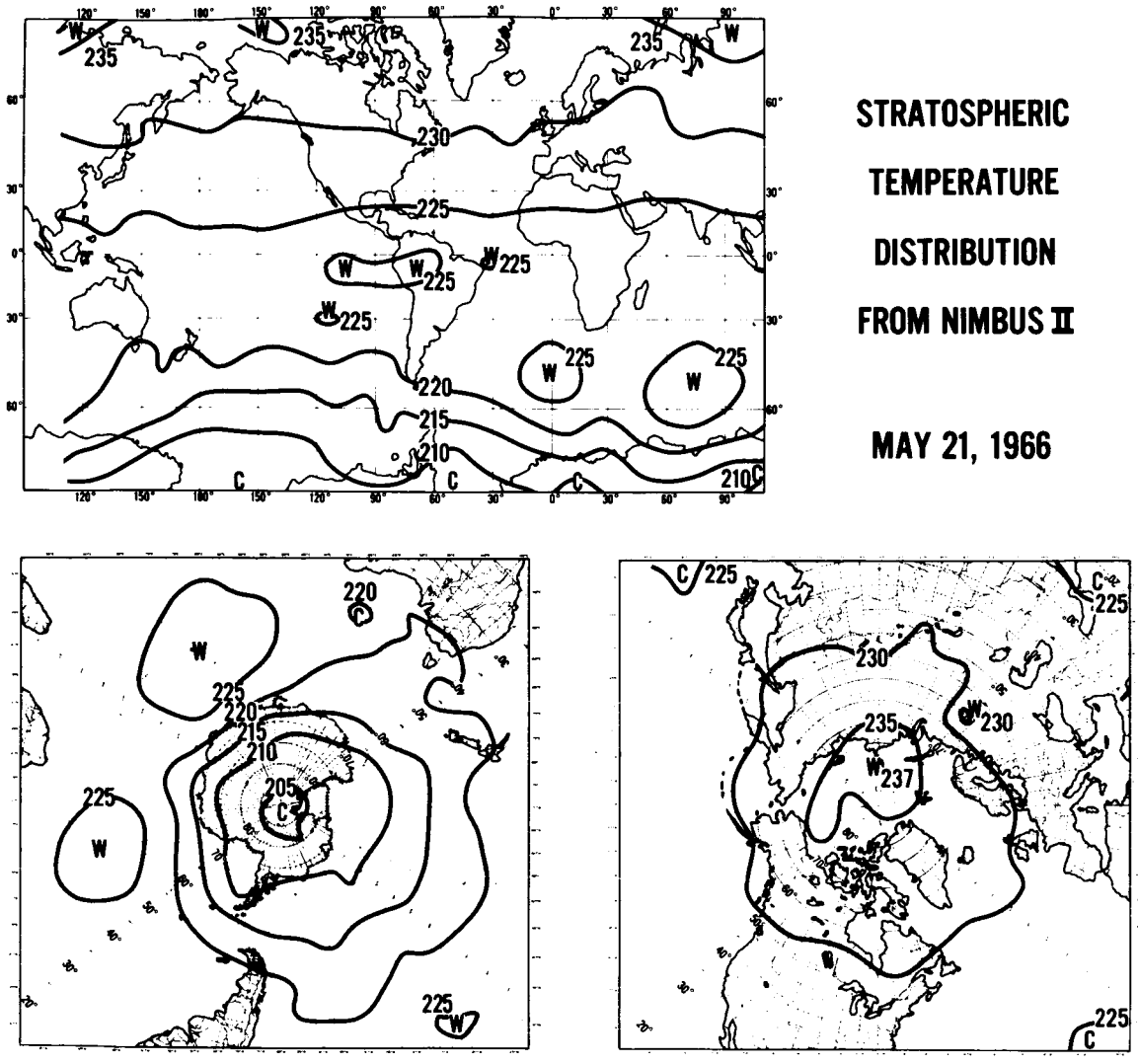

Figure 10. Global stratospheric temperature distribution (°K) on May 21, 1966.

mid-May the stratospheric temperature over central Antarctica dropped to 196°K at the beginning of July, but stayed almost isothermal throughout July. The maximum stratospheric cooling over the entire period (Figure 17) was not observed over the Antarctic continent within the polar night region but over the southern South Atlantic and Indian Ocean at 55° to 65°S. Figures 18 to 20 indicate that this cooling pattern was achieved by a distinct temperature wave which migrated around the South Pole over the higher mid-latitudes and showed a decreasing amplitude with time, almost vanishing during July. These findings from the satellite observations suggest an important role of dynamic processes in the

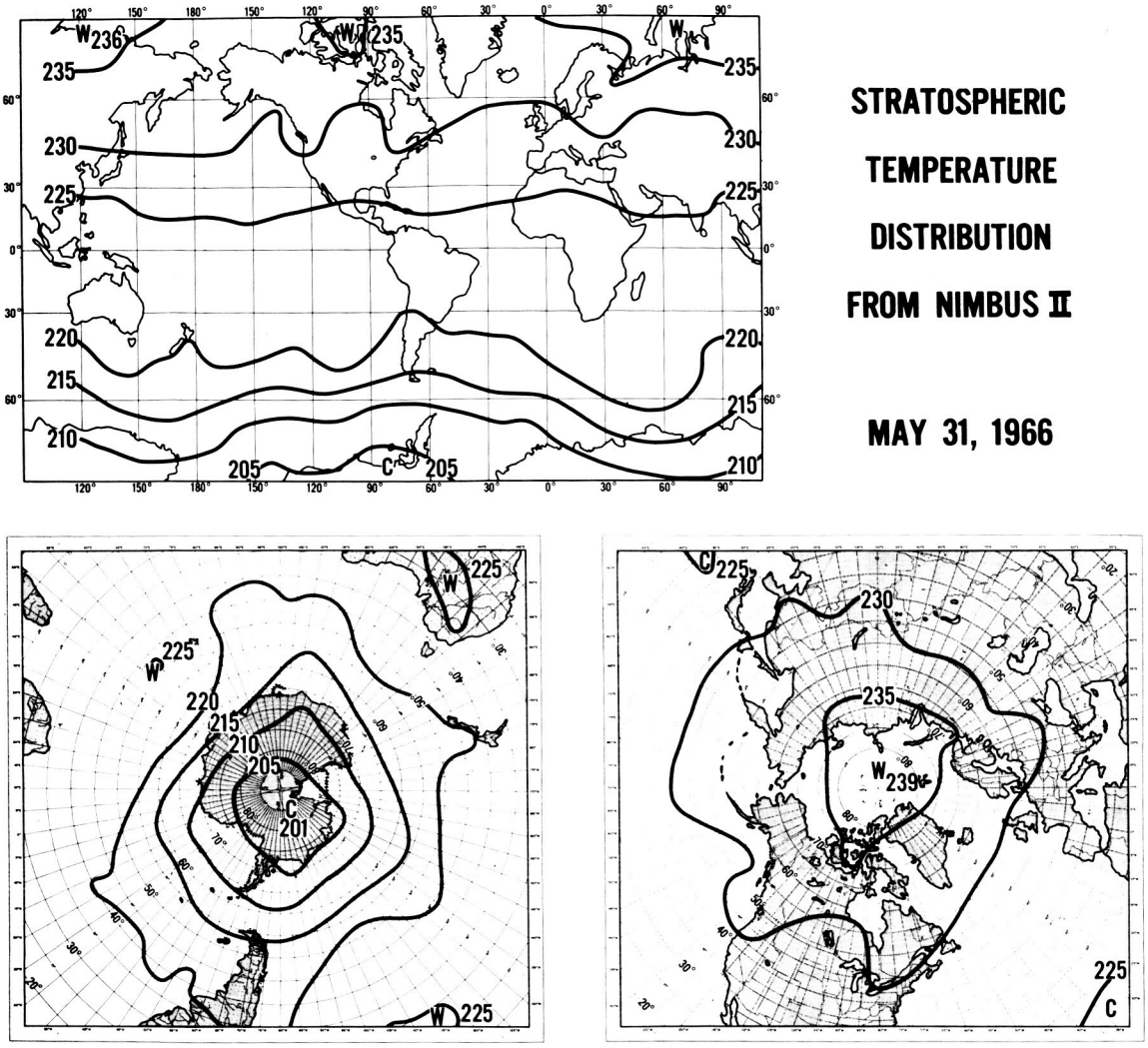

Figure 11. Global stratospheric temperature distribution (°K) on May 31, 1966.

winterly cooling pattern within the southern hemispheric stratospheric polar vortex. At least during the described experiment, these dynamic processes seem to exceed by far the mainly radiationally controlled cooling within the polar night regime.

CONCLUSIONS

The presented results of the Nimbus II medium resolution infrared radiometer experiment give new evidence that

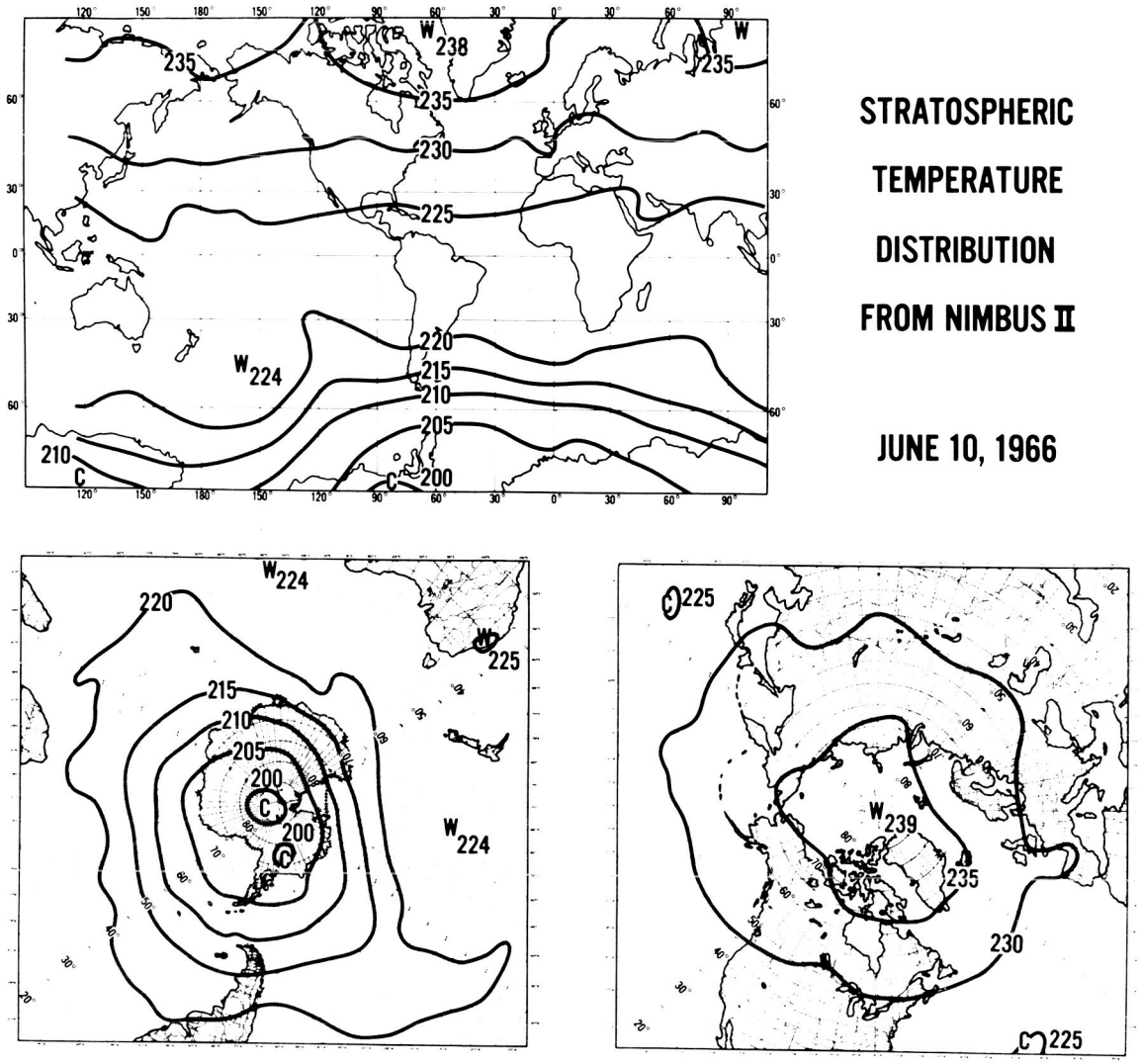

Figure 12. Global stratospheric temperature distribution (°K) on June 10, 1966.

(a) complete global data coverage can be achieved by a scanning radiometer in a quasi-polar orbit,

(b) radiometric measurements within the 15 micron carbon dioxide absorption band can provide a daily global survey of the horizontal distribution of vertical mean stratospheric temperature,

(c) the cloud influence on the 15 micron measurements can be eliminated by use of a theoretical correction model including "window"-channel radiometer measurements,

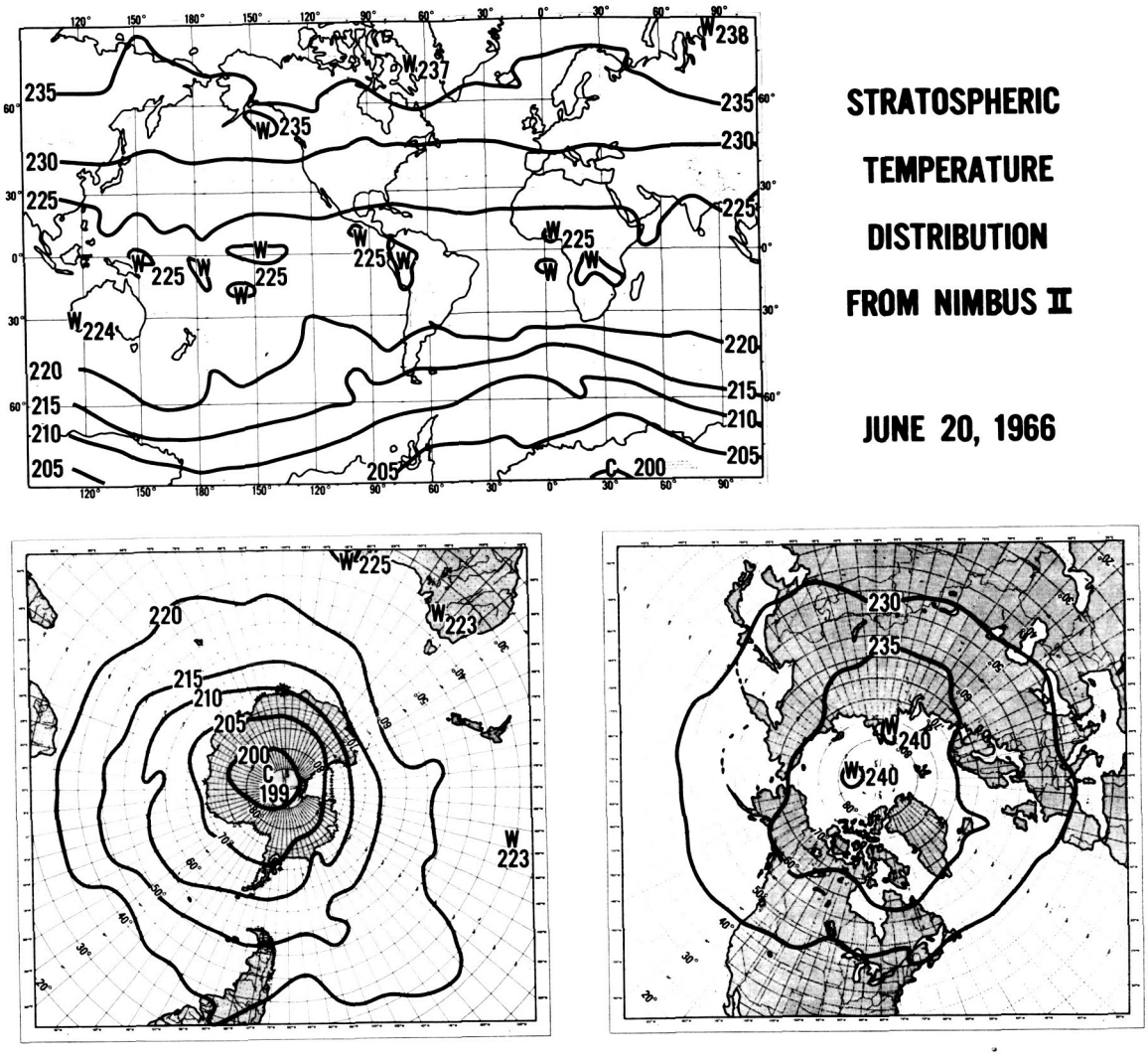

Figure 13. Global stratospheric temperature distribution (°K) on June 20, 1966.

(d) significant circulation features of the stratosphere can be derived from the obtained temperature patterns. This is of particular importance for large areas of the world, like the oceans and the polar regions, where a serious lack of stratospheric information exists.

The TIROS VII and the Nimbus II experiments have established a minimum limiting spectral width (with the attendant low signal-to-noise ratio) and a maximum limiting spectral width (with accompanying interference due to high clouds), respectively, with regard to the interpretability of the 15 micron measurements in terms of stratospheric temperatures. Thus, future satellite experiments like

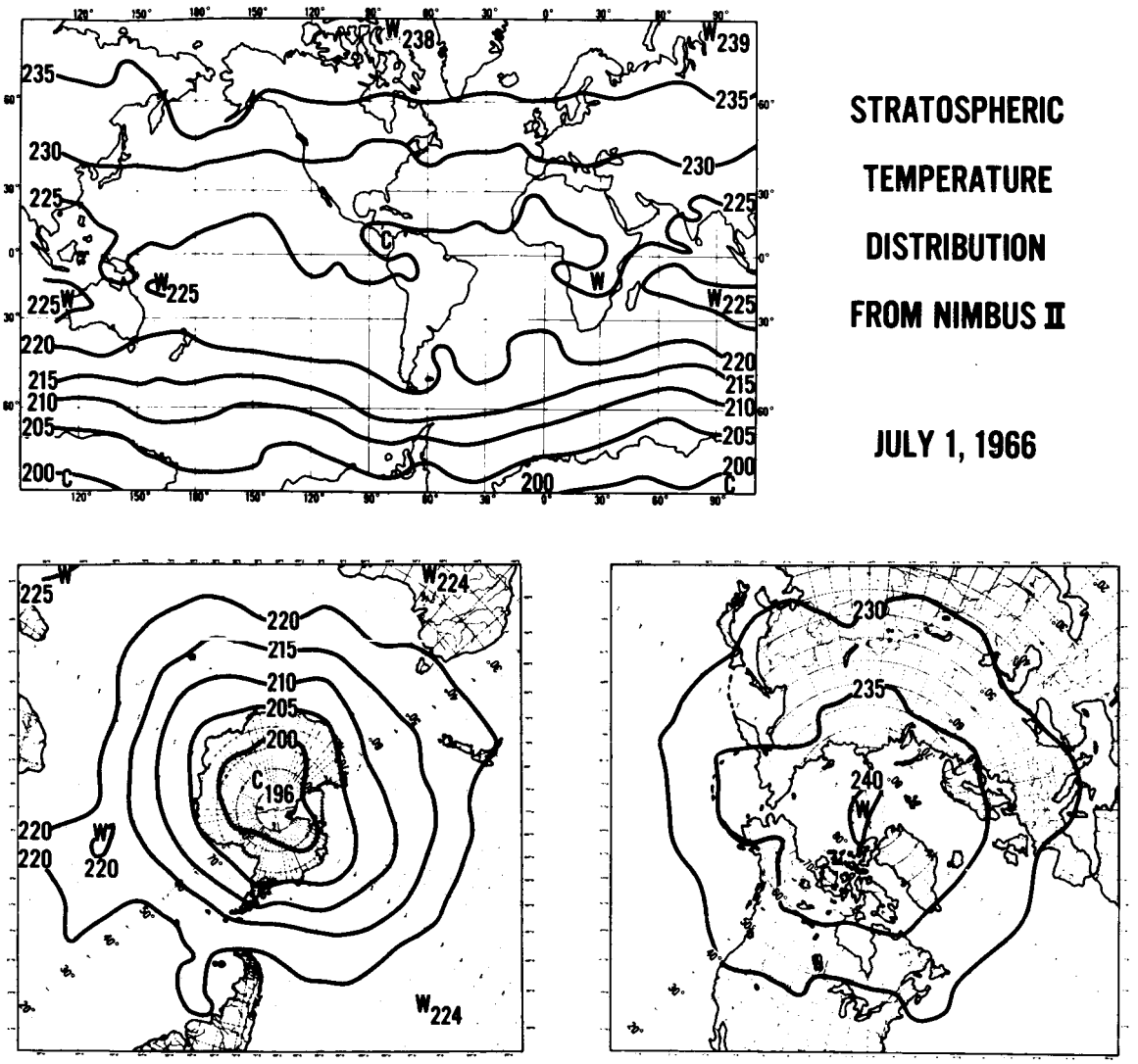

Figure 14. Global stratospheric temperature distribution (°K) on July 1, 1966.

the one to be flown on the forthcoming Nimbus B spacecraft will achieve a compromise between the signal-to-noise ratio and the cloud effect and bring the predominant part of the weighting function higher back into the stratosphere.

The described method of remote sensing of stratospheric temperatures including the data reduction system will not only have a valuable potential for stratospheric research but might become of essential importance when real-time global stratospheric temperature observations are required for the forthcoming supersonic transport operations in the next decade.

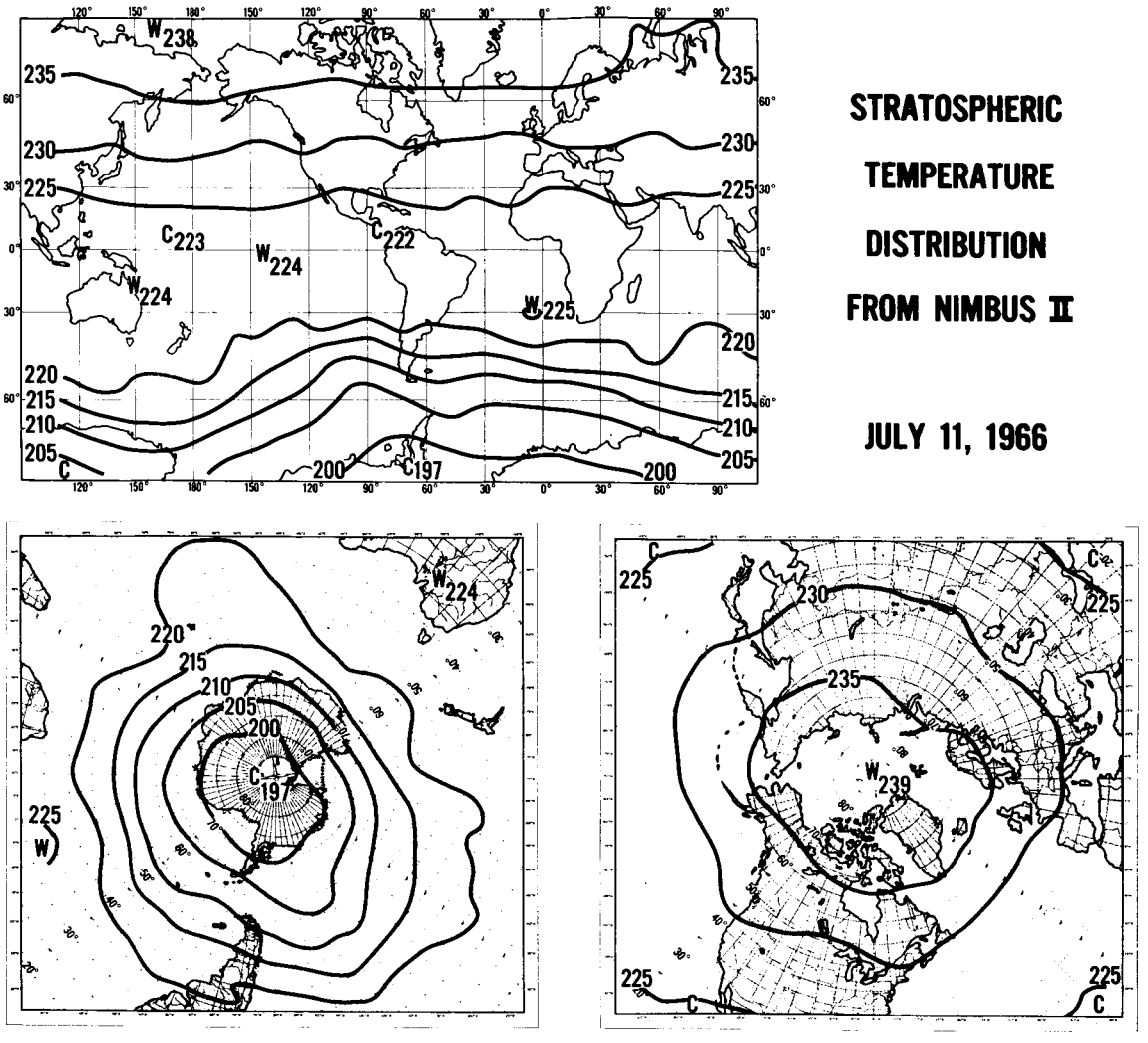

Figure 15. Global stratospheric temperature distribution (°K) on July 11, 1966.

ACKNOWLEDGMENTS

The author is indebted to the experimenter, Mr. Andrew W. McCulloch, as well as Mr. W. R. Bandeen, Mr. Virgil G. Kunde, and Mr. Robert Hite of the Planetary Radiations Branch, Goddard Space Flight Center, for support and assistance in accomplishing the basic material for this presentation. In addition I wish to thank Mr. Hugh W. Powell of the Computer Application, Inc. for his excellent programming efforts on behalf of this project.

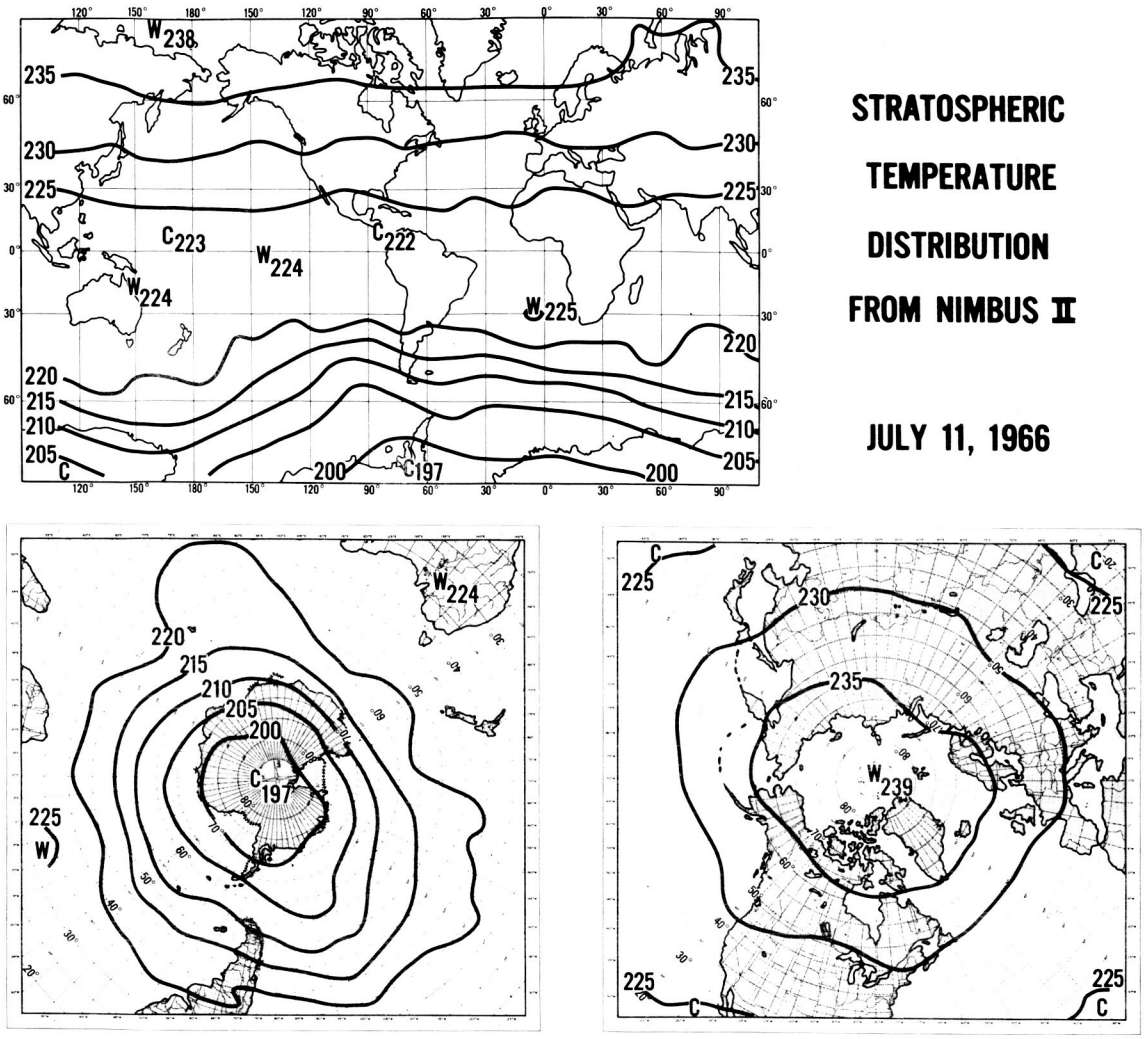

Figure 15. Global stratospheric temperature distribution (°K) on July 11, 1966.

ACKNOWLEDGMENTS

The author is indebted to the experimenter, Mr. Andrew W. McCulloch, as well as Mr. W. R. Bandeen, Mr. Virgil G. Kunde, and Mr. Robert Hite of the Planetary Radiations Branch, Goddard Space Flight Center, for support and assistance in accomplishing the basic material for this presentation. In addition I wish to thank Mr. Hugh W. Powell of the Computer Application, Inc. for his excellent programming efforts on behalf of this project.

3. Nordberg, W., McCulloch, A. W., Foshee, L. L., Bandeen, W. R., "Preliminary Results from Nimbus II" Bull. Amer. Meteor. Soc., Vol. 47, No. 11, pp. 857-872, (1966).

4. Kaplan, L. D., "Interference of Atmospheric Structure from Remote Radiation Measurements," Journal. Opt. Soc. Amer., Vol. 49, pp. 1004-1007, (1959).

5. Nimbus Project, "Nimbus II Users' Guide," Goddard Space Flight Center, Greenbelt, Md.

6. Kunde, V., "Theoretical Computations of the Outgoing Infrared Radiance from a Planetary Atmosphere," National Aeronautics and Space Administration, Washington, D. C. NASA TN D-4045 (1967).

7. Kennedy, J. S. "An Atlas of Stratospheric Mean Isotherms Derived from TIROS VII Observations" Goddard Space Flight Center, Greenbelt, Md., Publ. X-622-66-307 (1966).

8. Kennedy, J. S., Nordberg, W., "Circulation Features of the Stratosphere Derived from Radiometric Temperature Measurements with the TIROS VII Satellite," Goddard Space Flight Center, Greenbelt, Md., Publ. X-620-67-134 (also accepted for publ. by Journal Atm. Science 1967).

9. Warnecke, G. "TIROS VII 15 Micron Radiometric Measurements and Mid-Stratospheric Temperatures" in: Satellite Data in Meteorological Research, National Center for Atmospheric Research, Boulder, Colorado NCAR-TN-11, pp. 215-228 (1966).

10. Warnecke, G., "The Utility of Satellite-Borne Radiometric Measurements for Stratospheric Research" in Proceedings of the Sixth Stanstead Seminar on the Middle Atmosphere, McGill University, Montreal, P.Q., Canada, Publication in Meteorology No. 80, pp. 285-292 (1966).

11. Warnecke, G., "Satelliten und Meteorologie," Annalen der Meteorologie, Deutscher Wetterdienst, Offenbach, Germany, 'Tagungsbericht Muenchen 1966' (in print).

12. Nimbus Project, "The Nimbus II Medium Resolution Infrared Pictorial Data Catalog," Goddard Space Flight Center, Greenbelt, Md. (1967).

13. Raschke, E. and Bandeen, W. R., "A Quasi-Global Analysis of Tropospheric Water Vapor Content from TIROS IV Radiation Data," Journ. Appl. Meteorol., Vol. 6, No. 3, pp. 468-481 (1967).

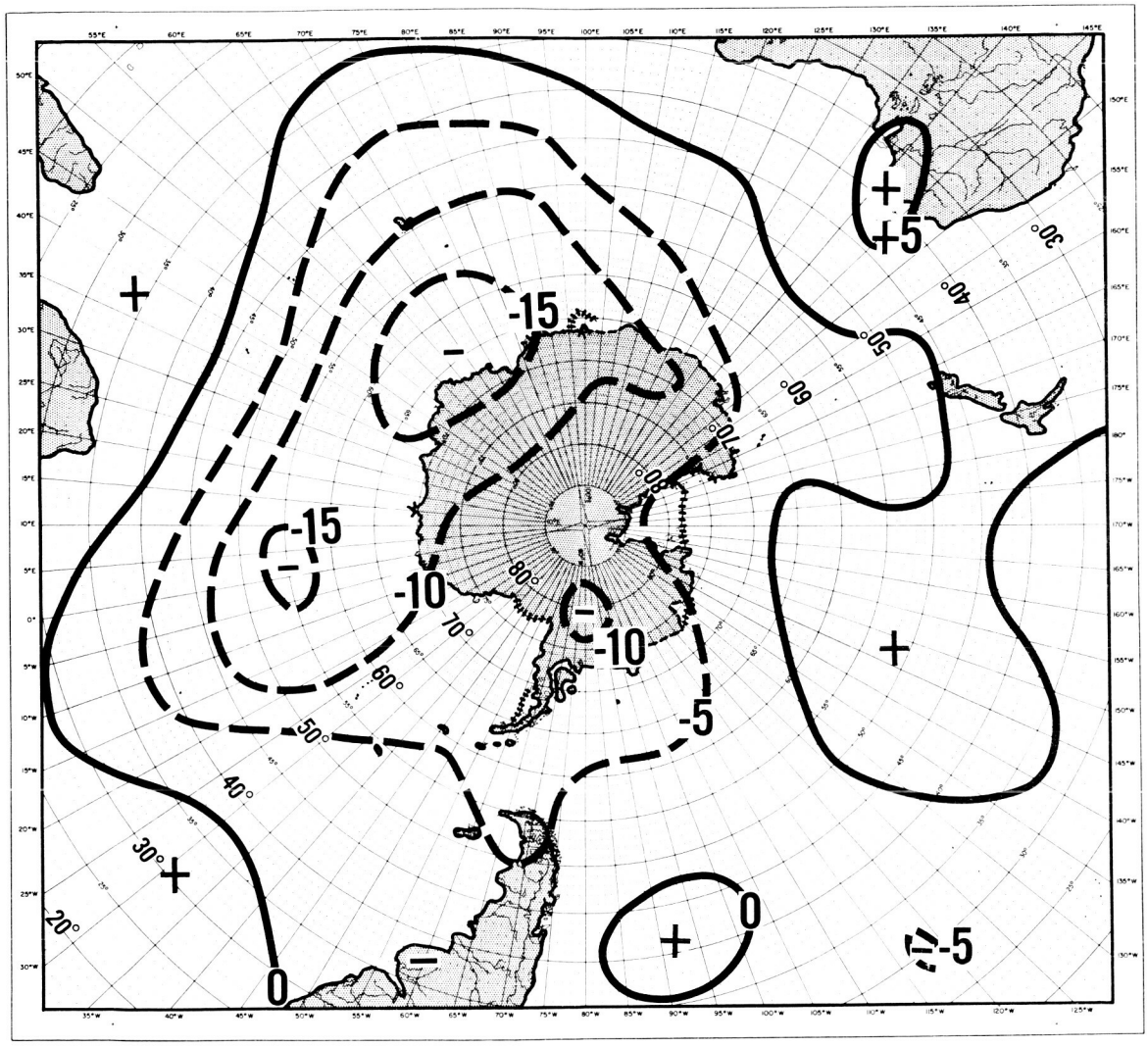

Figure 17. Stratospheric temperature change over the southern hemisphere (in °K) from May 21 to July 24, 1966.

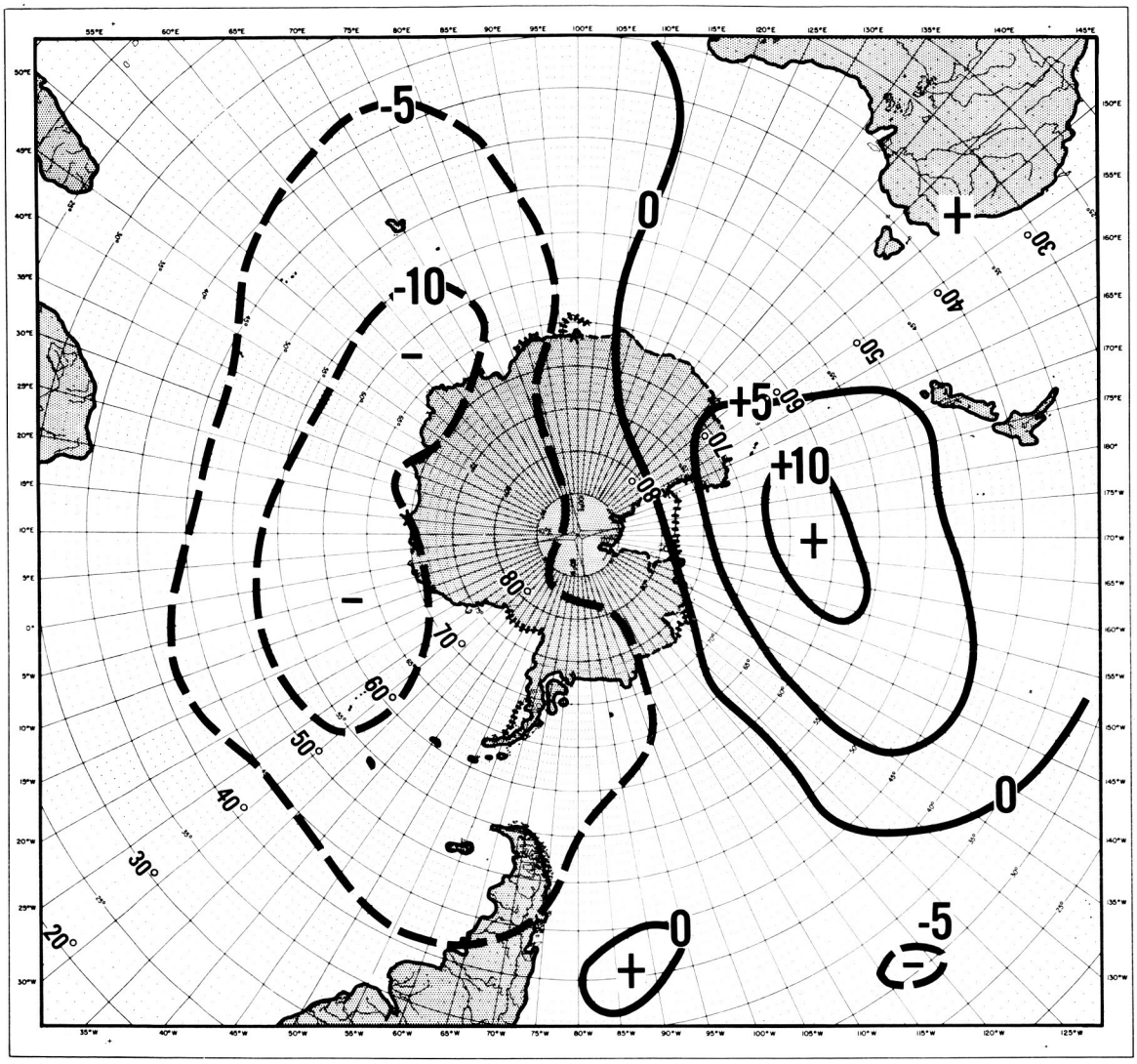

Figure 18. Stratospheric temperature change over the southern hemisphere (in °K) from May 21 to June 10, 1966.

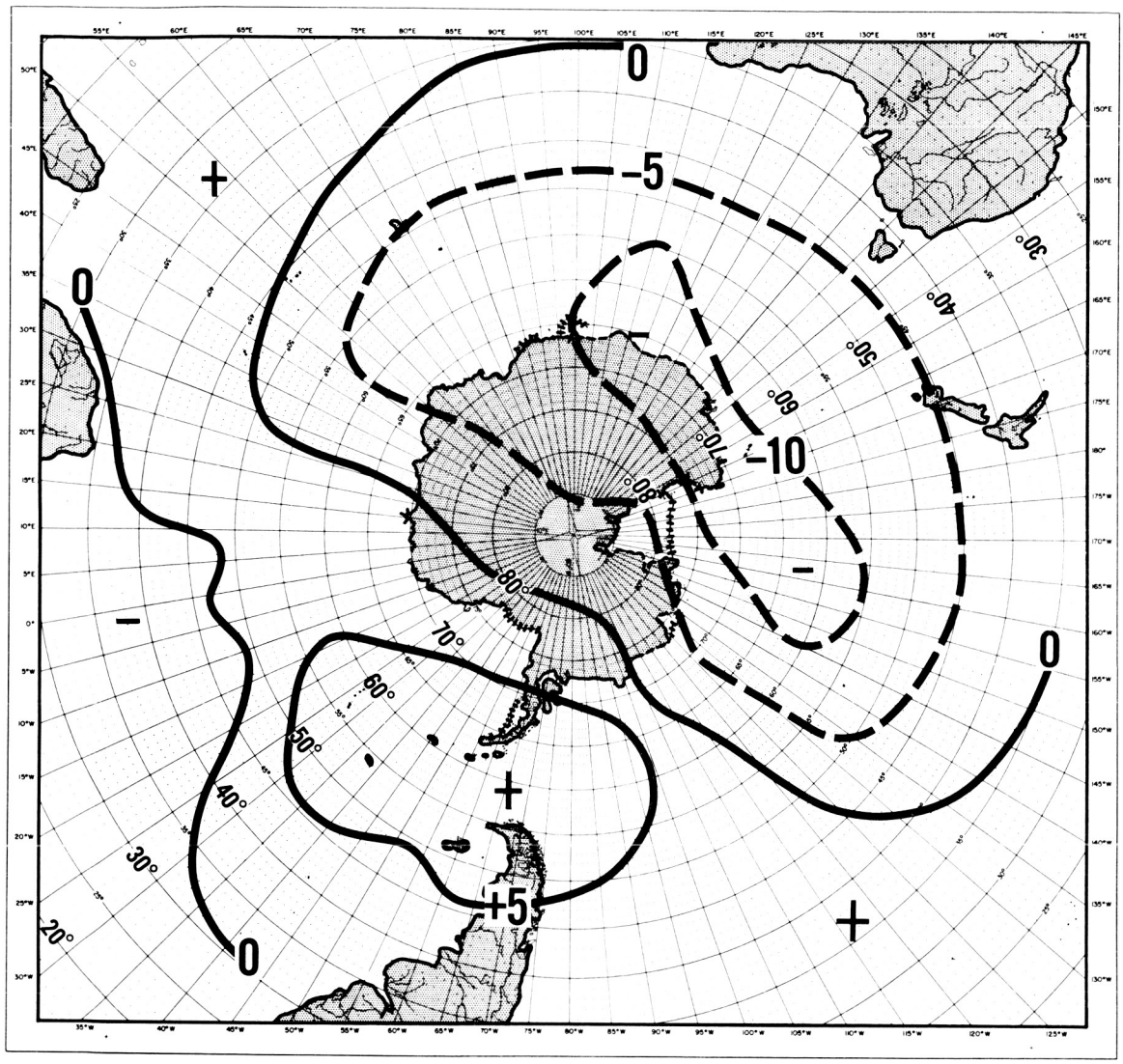

Figure 19. Stratospheric temperature change over the southern hemisphere (in °K) from June 10 to July 1, 1966.

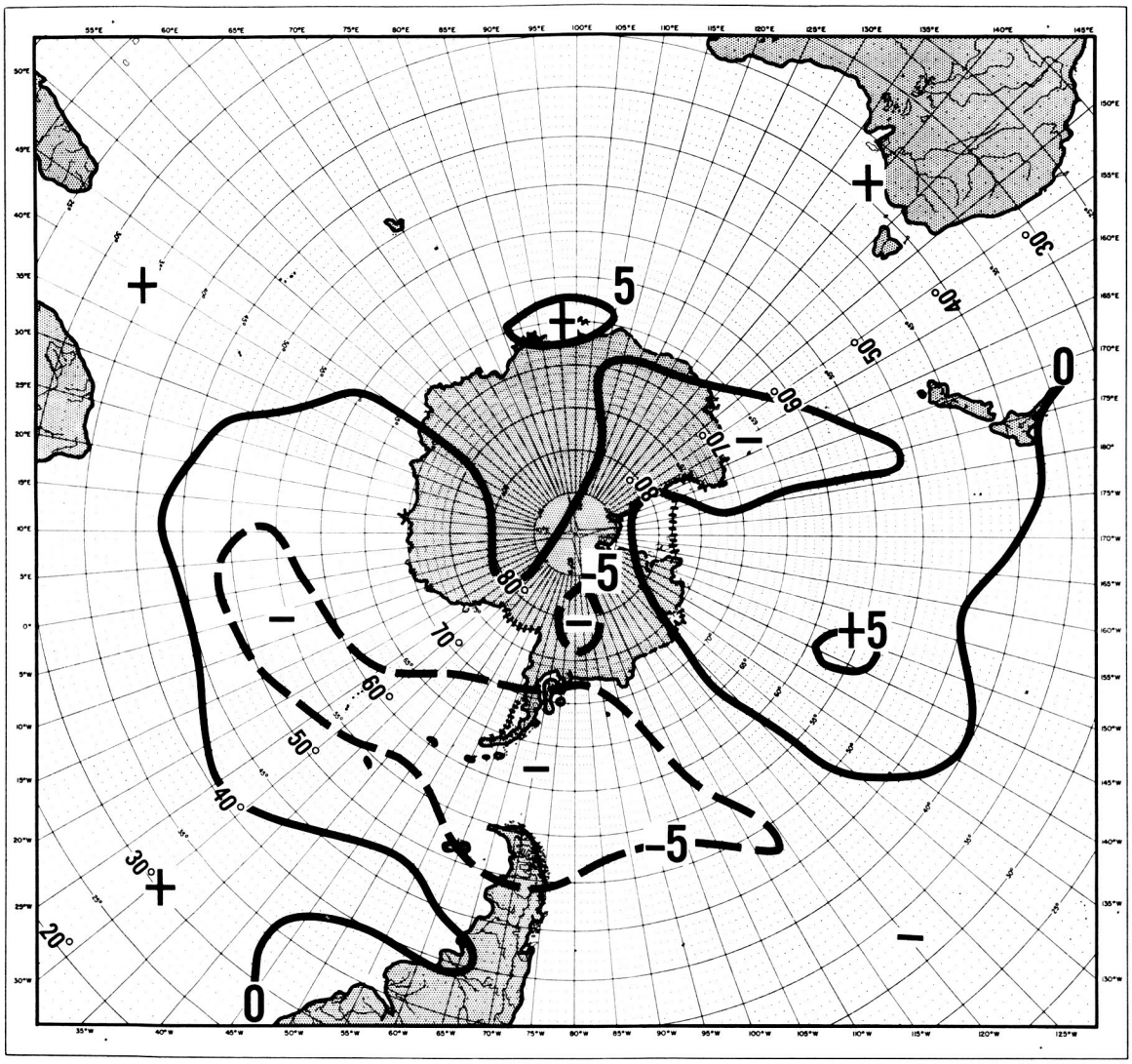

Figure 20. Stratospheric temperature change over the southern hemisphere (in °K) from July 1 to July 24, 1966.